

On Learning, Uncertainty and Synchronization in Stochastic Neural Ensembles

Jake Bouvrie (jvb@math.duke.edu)

Department of Mathematics, Duke University, Durham, NC USA

Jean-Jacques Slotine (jjs@mit.edu)

Nonlinear Systems Laboratory, Massachusetts Institute of Technology, Cambridge, MA USA

Abstract

We consider learning in coupled stochastic neural ensembles obeying a nonlinear gradient dynamics, where the task for the neural population is to learn a decision function in the presence of noise. Given that there is noise corrupting the learning process, how can one assign a confidence to the predictions of such a function and how can the organism reduce uncertainty in its decisions? In this paper we explore quantitatively the role of synchronization in determining uncertainty in neural learning. We show that uncertainty can be controlled in large part by trading off coupling strength among multiple neural populations against the noise amplitude. The impact of the coupling strength is quantified by the spectrum of the network Laplacian, and we discuss the role of network topology in synchronization and in reducing the effect of noise. Simulations comparing theoretical bounds to the relevant empirical quantities show that the estimates can be tight.

Keywords: Stochastic dynamics, gradient dynamics, learning, synchronization, stochastic contraction, neural uncertainty, neural decision making, population coding, collective enhancement.

1 Introduction

Motivated by the problem of learning to discriminate in the brain, we consider a population of neurons whose goal is to learn a decision function by implementing a nonlinear gradient dynamics. The dynamics, however, are assumed to be corrupted by perturbations modeling noise intrinsic to the neural environment (Faisal et al., 2008). If there is noise corrupting the learning process, an immediate question is whether it is possible to assign a confidence to the predictions of the learned function, and whether (and to what extent) the organism can reduce uncertainty in its decisions by taking advantage of a ubiquitous mechanism such as synchronization and/or averaging. Indeed, it is a well known fact that synchrony within a system of coupled dynamical elements provides robustness to perturbations occurring in any one element’s dynamics (Needleman et al., 2001; Wang and Slotine, 2005; Pham and Slotine, 2007). One reasonable sounding solution is to suppose that there are multiple *copies* of the neural learning circuit (Adams, 1998; Fernando et al., 2010), and that averaging over the different solutions might reduce noise via cancelation effects. This solution will unfortunately rarely work because when the dynamics followed by the different dynamical systems are nonlinear, one cannot expect to gain a meaningful signal by linear averaging (Tabareau et al., 2010). As neurons are susceptible to saturation of their firing rates, the macroscopic dynamics that neuron populations obey can be strongly nonlinear. It is reasonable however to suppose that *synchronization* across neuron populations may provide sufficient phase alignment to make linear averaging, and thus “consensus”, a powerful proposal (Tabareau et al., 2010; Cao et al., 2010; Young et al., 2010; Poulakakis et al., 2010; Gigante et al., 2009).

In this paper we explore quantitatively the role of synchrony in controlling uncertainty arising from the noise. In particular, we base our work on the argument that noisy, nonlinear trajectories can be linearly averaged if fluctuations due to noise can be made small and that fluctuations can be made small by coupling the

dynamical elements. In the stochastic setting adopted here, synchronization should be understood as a tendency for individual elements’ trajectories to move towards a common trajectory, in a quantifiable sense. The estimates we present directly characterize the tradeoff between the network’s tendency towards synchrony and the ambient neuronal noise, and ultimately address the specific role this tradeoff plays in determining uncertainty surrounding a function learned by a noisy population of nonlinear neurons.

We further show how and where the topology of the network of neural ensembles impacts the extent to which the noise, and therefore uncertainty, can be controlled. The estimates we provide take into account in a fundamental way both the nonlinearity in the dynamics and the noise, and are novel contributions to the best of our knowledge. More generally, the work discussed here also has implications in other related domains, such as networks of coupled learners or adaptive sensor networks, and can be extended to multitask online or dynamic learning settings. The difficulty inherent in analyzing *dynamic* learning systems, such as hierarchies with feedback (Mumford, 1992; Lee and Mumford, 2003), poses a challenge. But considering dynamic systems can yield substantial benefits: transients can be important, as suggested by the literature on regularization paths and early stopping (Yao et al., 2007). Furthermore, the role of feedback/backprojections and attention-like mechanisms in learning and recognition systems, both biological and artificial, is known to be important but is not well understood (Hahnloser et al., 1999; Itti and Koch, 2001; Hung et al., 2005).

The paper is organized as follows. In Section 2 we setup the learning problem and define an appropriate system of stochastic differential equations (SDEs) modeling a simple dynamic learning process. We then discuss stability and network topology in the context of synchronization. In Section 3 we present the main results of the paper, a set of uncertainty estimates, postponing technical details until later. Then in Section 5 we provide simulations and compare empirical estimates to the theoretical quantities predicted by the Theorems in Section 3. Section 4 provides a discussion addressing the significance and applicability of our theoretical contributions to neuroscience and behavior. Finally, in Section 6 we give proofs of the results stated in Section 3.

2 Biological Learning in a Stochastic Network

For simplicity we consider a simple, linear learning problem in one dimension described by a square loss objective, in the spirit of Rao & Ballard (Rao and Ballard, 1999). This setting also supports nonlinear decision functions in the sense that we might consider taking a linear function of nonlinear variables whose values might be computed upstream. In this case the development would be similar, but extended to the multidimensional case. The development may also be extended to richer function classes and more exotic loss functions directly, however for our purposes the additional generality does not contribute constructively to our primary goals and furthermore might raise biological plausibility concerns¹.

2.1 Problem Setup

Assume that we have observed a set of examples $\{x_i \in \mathbb{R}, y_i \in \mathbb{R}\}_{i=1}^m$, each representing a unit of sensory experience, and want to estimate the linear regression function $f_w(x) = wx$. Adopting the square loss, the total error incurred on the observations by f_w is given by

$$E(w) = \sum_{i=1}^m (y_i - f_w(x_i))^2 = \sum_{i=1}^m (y_i - wx_i)^2.$$

We will model adaptation of the neuron’s weights (training) by a noisy gradient descent process, with biologically plausible dynamics, on this squared prediction error loss function. The parameter’s trajectory over time $w(t)$ and its governing dynamics may be interpreted as describing a stochastic rate code, or average activity in a population of neurons. The dynamical system may also be interpreted as modeling the noisy, time-varying strength of a local field potential or other macro electrophysiological signal. We will discuss the latter possibility in Section 4.

The gradient of E with respect to the weight parameter is given by $\nabla_w E = -\sum_{i=1}^m (y_i - wx_i)x_i$, however the gradient dynamics $\dot{w} = -\nabla_w E(w)$ are implausible for two important reasons:

¹In the sense that one would have to carefully justify biologically the particular nonlinearities going into a nonlinear decision function on a case-by-case basis.

1. The gradient can only be represented up to finite magnitude before *saturation* occurs.
2. The presence of often substantial *noise* has been ignored.

We can work with a more realistic dynamics which include saturation effects by saturating the gradient, $\dot{w} = -\tanh(a\nabla_w E(w))$, where a is a slope parameter, and model the noise with an additional diffusion term giving the SDE

$$dw_t = -\tanh(a\nabla_w E(w_t))dt + \sigma dB_t, \quad (1)$$

where dB_t denotes the standard 1-dimensional Wiener increment process and $\sigma > 0$. Here, the noise term σdB_t corresponds to intrinsic neuronal noise (Faisal et al., 2008) but can more generally model measurement error in networks of coupled dynamical elements.

2.2 Synchronization and Noise

Suppose now that one takes n independent copies of the neural circuit implementing the dynamics (1), with associated parameters $\{w_1(t), \dots, w_n(t)\}$. Since these dynamics are nonlinear, we cannot hope to reduce the effect of the noise by simply averaging over the independent trajectories. However, if the circuit copies are coupled strongly enough they will attempt to *synchronize*, and averaging over the copies becomes a potentially powerful way to reduce the effect of the noise (Sherman and Rinzel, 1991; Needleman et al., 2001). In the present setting the noise can be large and will of course act to break the synchrony. We will explore how well the noise can be reduced by synchronization in the following sections.

Given n *diffusively* coupled copies of the noisy neural circuit and setting $a = 1$ in (1), we have the following system of nonlinear SDEs:

$$dw_i(t) = -\tanh\left[\sum_{\ell=1}^m (w_i(t)x_\ell - y_\ell)x_\ell\right]dt + \sum_{j=1}^n W_{ij}(w_j - w_i)dt + \sigma dB_t^{(i)} \quad (2)$$

for $i = 1, \dots, n$, where $B_t^{(i)}$ are *independent* standard Wiener processes. Diffusive couplings model electrical connections such as those implemented by gap junctions in the mammalian brain (Fukuda et al., 2006; Bennett and Zukin, 2004). Each circuit copy is corrupted by independent noise processes but follows the same noise-free dynamics as the others. We will assume for simplicity uniform symmetric weights $W_{ji} = W_{ij} = \kappa > 0$ when element i is connected to element j . Note that we might consider these coupled systems each starting from very different initial conditions. Defining $(\mathbf{w})_i$ to be the (scalar) output of the i -th circuit, we can rewrite the system (2) in vector form as

$$d\mathbf{w}(t) = -\left(\tanh\left[\sum_{i=1}^m (\mathbf{w}(t)x_i - y_i\mathbf{1})x_i\right] + L\mathbf{w}(t)\right)dt + \sigma d\mathbf{B}_t \quad (3)$$

where $L = \text{diag}(W\mathbf{1}) - W$ is the *network Laplacian*, and \mathbf{B}_t is the standard n -dimensional Wiener process. The spectrum of the network Laplacian captures important properties of the network's topology, and will play a key role in the remainder of the paper. Finally, the change of variable $X_t := \mathbf{w}\|\mathbf{x}\|^2 - \langle \mathbf{x}, \mathbf{y} \rangle \mathbf{1}$, with $(\mathbf{x})_i = x_i, (\mathbf{y})_i = y_i$, yields a system that will be easier to analyze:

$$dX_t = -(\tanh(X_t)\|\mathbf{x}\|^2 + LX_t)dt + \tilde{\sigma}d\mathbf{B}_t \quad (4)$$

where we have defined $\tilde{\sigma} := \sigma\|\mathbf{x}\|^2$. The unique globally stable equilibrium point for the deterministic part of (4) is seen to be $X^* = 0$, which checks with the fact that the solution to the linear regression problem is $w^* = \langle \mathbf{x}, \mathbf{y} \rangle / \langle \mathbf{x}, \mathbf{x} \rangle$ in this simple case.

2.3 Role of Network Topology

In this section we briefly consider the role of network topology in controlling uncertainty by way of controlling synchronization properties. The graphs discussed here will be helpful examples to keep in mind when interpreting the results given in Section 3. The topology of the network of neurons can be seen to influence

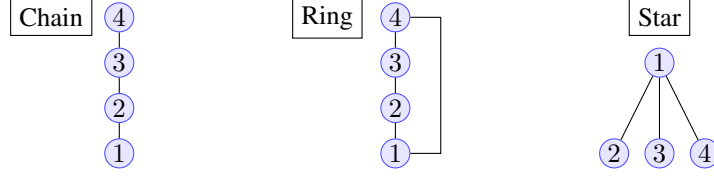


Figure 1: *Examples of (undirected) network graphs.*

the robustness of synchrony to noise through the spectrum of the Laplacian, and plays an important role in synchronization of dynamical systems more generally (Kopell and Ermentrout, 1986; Kopell, 2000; Jadbabaie et al., 2003; Wang and Slotine, 2005; Taylor et al., 2009; Poulakakis et al., 2010). The simplest graph of coupled elements is perhaps the full, all-to-all graph. As one can imagine, this network is also the easiest to synchronize as each element can speak directly to all the others. Although n^2 connections has been criticized as being biologically unrealistic, all-to-all connectivity can be implemented with $2n$ connections using, for example, quorum sensing ideas (Taylor et al., 2009), where a global average is computed and shared or simply sensed chemically. Regardless of how the full graph is implemented, the spectrum of the combinatorial Laplacian L for this graph shows why it might be especially effective for reducing uncertainty in the context of Equation (3). With uniform coupling strength $\kappa > 0$, one can check that $\lambda(L) = \{0, n\kappa, \dots, n\kappa\}$. Denote by λ_- the smallest non-zero (Fiedler) eigenvalue, and by λ_+ the largest eigenvalue. Here, $\lambda_- = \lambda_+ = n\kappa$ and as we will show below in Theorem 3.1, the effect of the noise can be reduced particularly quickly when both κ and n are increased.

As fewer connections are made in the network, it becomes harder to synchronize, and we move away from the all-to-all ideal. Figure 1 shows some other common network graphs. The undirected ring graph, appearing in the middle, has spectrum $\lambda_i(L) = 2\kappa [1 - \cos(\frac{2\pi}{n}(i-1))], i = 1, \dots, n$. If the single edge connecting the first and last elements is removed to make a chain as shown on the left in the Figure, the network becomes considerably harder to synchronize (Kopell and Ermentrout, 1986), although the spectrum of the chain looks similar: $\lambda_i(L) = 2\kappa [1 - \cos(\frac{\pi}{n}(i-1))]$. Finally, the star graph shown on the right in the Figure has spectrum $\lambda(L) = \{0, \kappa, \dots, \kappa, n\kappa\}$, and we can see immediately that since the Fiedler eigenvalue $\lambda_- = \kappa$ does not grow with the size of the network. The Theorems in Section 3 then predict that it will be impossible to increase the synchronization rate simply by incorporating more copies of the neural circuit. The coupling strength must also increase to make fluctuations from the center of mass small. We will discuss this case in more detail below. As might be particularly relevant to brain anatomy, random graphs and directed graphs may also be considered but are beyond the scope of this work.

2.4 A Comment on Stability and Contraction

We turn to analyzing the stability of the nonlinear system given by Equation (4). We will argue that this is difficult for two reasons: the noise, and the fact that the (noise-free) dynamics saturate in magnitude. Indeed, without additional assumptions, one can not in general show that the system is globally exponentially stable. A common method for studying the stability properties of a noiseless nonlinear dynamical system is via Lyapunov theory (Slotine and Li, 1991), however in the presence of noise system trajectories along the Lyapunov surface may not be strictly decreasing. Contraction analysis (Lohmiller and Slotine, 1998; Wang and Slotine, 2005) is a differential formalism related to Lyapunov exponents, and captures the notion that a system is stable in some region if initial conditions or temporary disturbances are forgotten. If all neighboring trajectories converge to each other, global exponential convergence to a single trajectory can be concluded:

Definition 2.1 (Contraction). *Given the system equations $\dot{\mathbf{x}} = \mathbf{f}(\mathbf{x}, t)$, a region of the state space is called a contraction region if the Jacobian $J_f = \frac{\partial \mathbf{f}}{\partial \mathbf{x}}$ is uniformly negative definite in that region. Furthermore, the contraction rate is given by β , where $\frac{1}{2}(J_f + J_f^T) \leq \beta \mathbf{I} < 0$.*

An analogous definition in the case stochastic dynamics has also been developed (Pham et al., 2009), and requires contraction of the noise-free dynamics as well as a uniform upper bound on the variance of the noise. However for the system (4), the Jacobian is found to be $J(\mathbf{w}) = \|\mathbf{x}\|^2 \text{diag}(\tanh^2(\mathbf{w}) - 1) - L$ so that $\lambda(J(\mathbf{w})) < -\lambda(L) \leq -\lambda_{\min}(L) = 0$. The subspace of constant vectors is a flow invariant

subspace, and L does not contribute to the dynamics in this flow invariant space since L has a zero eigenvalue corresponding to its constant eigenvector. This difficulty arises whenever one considers diffusively coupled elements, and in such cases the usual way around this difficulty is to work with an auxiliary or virtual system (as in e.g. (Pham and Slotine, 2007)) and study contraction to the flow invariant subspace starting from initial conditions outside. However since $\tanh'(x) = 1 - \tanh^2(x)$, we still are left with the difficulty that the noise-free dynamics can have a convergence rate to equilibrium arbitrarily close to zero as one travels far out to the tails of the \tanh function; the system is not necessarily contracting. Indeed, for any saturated dynamics, $\tanh(\mathbf{f}(\mathbf{x}, t))$, the rate can be arbitrarily small. Thus one cannot easily determine the rate of convergence to equilibrium using standard techniques. The analysis which we provide in the succeeding sections will attempt to get around these difficulties by separately exploring the system's behavior in and out of the flow-invariant subspace of constant vectors.

3 Characterizing Uncertainty

In this section we present and interpret the main results of the paper. The argument we put forward is that noisy, nonlinear trajectories can be linearly averaged to reduce the noise if fluctuations due to noise can be made small. We show that the fluctuations can be made small by coupling the dynamical elements, and that one can precisely control the size of the fluctuations. In particular, we give estimates which show that the tradeoff between noise and coupling strength among neuron populations determines the amount of uncertainty surrounding the decisions made by the circuit. Proofs of the Theorems are postponed until Section 6.

3.1 Preliminaries

We begin by decomposing the stochastic process $\{X_t \in \mathbb{R}^n\}_{t \geq 0}$ into a sum describing fluctuations about the center of mass. Let $P = I - (1/n)\mathbf{1}\mathbf{1}^\top$, the canonical projection onto the zero-mean subspace of \mathbb{R}^n , and define $Q = I - P$. Then for all $t \geq 0$, $X_t = PX_t + QX_t$. Clearly, $\ker P = \text{im } Q$ is the subspace of constant vectors. We will adopt the notation \tilde{X}_t for PX_t , and $\bar{X}_t\mathbf{1}$ for QX_t (along with the analogous notation $\tilde{\mathbf{w}}_t$ and \bar{w}_t), and derive expressions for these quantities based on Equation (4). The macroscopic variable \bar{X}_t satisfies

$$d\bar{X}_t = \frac{1}{n}\mathbf{1}^\top dX_t = -\frac{\|\mathbf{x}\|^2}{n}\mathbf{1}^\top \tanh(X_t)dt + \frac{\tilde{\sigma}}{\sqrt{n}}dB_t \quad (5)$$

and thus

$$d\tilde{X}_t = dX_t - d\bar{X}_t\mathbf{1} = -\left(\tanh(X_t)\|\mathbf{x}\|^2 + LX_t - \frac{\|\mathbf{x}\|^2}{n}\mathbf{1}^\top \tanh(X_t)\mathbf{1}\right)dt + \tilde{\sigma}d\mathbf{B}_t - \frac{\tilde{\sigma}}{\sqrt{n}}dB_t\mathbf{1}. \quad (6)$$

In terms of the original variable \mathbf{w} , the fluctuations $\tilde{\mathbf{w}}_t$ are purely due to the noise, while \bar{w}_t parameterizes the average decision function. As the decision function we consider is linear, the uncertainty in the decisions is directly equivalent to uncertainty in the parameter w . We will study the evolution of both the mean and the fluctuation processes over time, however to assess uncertainty the central quantity of interest will be the size of the ball containing the fluctuations (the ‘‘microscopic’’ variables). We characterize the magnitude of the fluctuations via the squared norm process satisfying

$$\frac{d\|\tilde{X}_t\|^2}{2} = -\left(\|\mathbf{x}\|^2\langle\tilde{X}_t, \tanh(X_t)\rangle + \langle\tilde{X}_t, LX_t\rangle\right)dt + \frac{1}{2}\tilde{\sigma}^2(n-1)dt + \tilde{\sigma}\|\tilde{X}_t\|dB_t \quad (7)$$

which follows from (6) applying Ito's Lemma to the function $h(\tilde{X}_t) = \frac{1}{2}\langle\tilde{X}_t, \tilde{X}_t\rangle$ and the fact that $\langle\tilde{X}_t, d\mathbf{B}_t\rangle = \|\tilde{X}_t\|dB_t$ in law.

3.2 Uncertainty Estimates

The first –and central– result says that the ball centered at \bar{w} (the center of mass) containing the fluctuations can be controlled in expectation from above and below by the coupling strength and in some cases, the number of circuit copies, via the spectrum of the network Laplacian L . Whether it is because they are difficult

to obtain or because they're simply not useful for stability analysis, lower bounds are typically ignored in the dynamical systems literature. We have found, however, that such bounds can be derived and that control from below has proven to be useful for deriving further Theorems of the sort that follow below.

Let λ_+ be the largest eigenvalue of L , and let λ_- be the smallest non-zero eigenvalue of L .

Theorem 3.1 (Fluctuations can be made small). *After transients of rate $2\lambda_-$*

$$\frac{(n-1)\sigma^2}{2\lambda_+} \left(1 - \frac{\|\mathbf{x}\|^2}{\lambda_-}\right) \leq \mathbb{E}\|\tilde{\mathbf{w}}(t)\|^2 \leq \frac{(n-1)\sigma^2}{2\lambda_-}$$

where $\tilde{\mathbf{w}} = P\mathbf{w}(t)$.

Clearly the lower bound is informative only when $\lambda_- > \|\mathbf{x}\|^2$. While we do not explicitly assume any particular bound on the size of the examples $\|\mathbf{x}\|$, it is reasonable that $\lambda_- \gg \|\mathbf{x}\|^2$ since λ_- can depend on the number of circuits n and will always depend on the coupling strength κ which can be large in the case of, for example, gap junction mediated electrical connections (Bennett and Zukin, 2004).

In the next Theorem we give the variance of the fluctuations via a higher moment of $\|\tilde{\mathbf{w}}\|$. This result makes use of the lower bound in Theorem 3.1, and leads to a result that gives control of the fluctuations in probability rather than in expectation.

Theorem 3.2 (Variance of the trajectory distances to the center of mass). *After transients of rate $2\lambda_-$*

$$\text{var}(\|\tilde{\mathbf{w}}(t)\|^2) \leq \left(\frac{(n-1)\sigma^2}{2\lambda_-}\right)^2 \left(2 + \frac{4}{n-1}\right) - \left(\frac{(n-1)\sigma^2}{2\lambda_+}\right)^2 \left(1 - \frac{\|\mathbf{x}\|^2}{\lambda_-}\right)^2.$$

Chebyshev's inequality combined with Theorem 3.2 immediately gives the following Corollary.

Corollary 3.1. *After transients of rate $2\lambda_-$*

$$\mathbb{P}\left[\|\tilde{\mathbf{w}}(t)\|^2 - \mathbb{E}\|\tilde{\mathbf{w}}(t)\|^2 \geq \varepsilon\right] \leq \frac{\text{var}(\|\tilde{\mathbf{w}}(t)\|^2)}{\varepsilon^2}. \quad (8)$$

Since any connected network graph has non-trivial eigenvalues which depend on the uniform coupling strength κ , we see that for fixed n as $\kappa \rightarrow \infty$, $\text{var}(\|\tilde{\mathbf{w}}(t)\|^2) \rightarrow 0$. In the case of the all-to-all network topology, for example, the eigenvalues of L depend on both n and κ so that $\text{var}(\|\tilde{\mathbf{w}}(t)\|^2) = \mathcal{O}(\kappa^{-2})$ giving a power law decay of order $\mathcal{O}(\kappa^{-2}\varepsilon^{-2})$ on the right hand side of Equation (8) in Corollary 3.1.

For the final result we turn to estimating in expectation the steady-state average distance between the trajectories of the circuit copies and the noise-free solution. As we have argued in Section 2.4, the rate of convergence to equilibrium of the trajectories $w_i(t)$ can be arbitrarily small. Although from the Theorems above the fluctuations can be made small, one cannot in general make a similar statement about the center of mass \bar{w}_t process unless assumptions about the initial conditions are made (and by extension, the same holds true for the trajectories $w_i(t)$). Such an assumption would lead to control over the contribution of the tanh terms, and establishes a lower bound on the contraction rate. Rather than make a specific assumption however, we state a general result. We again provide a lower bound, this time following from the law of large numbers governing sums of i.i.d. Gaussian random variables and the lower bound on the fluctuations provided by Theorem 3.1.

Theorem 3.3 (Average distance to the noise-free trajectory). *Denote by w^* the minimizer of the squared-error objective (2.1). After transients of rate $2\lambda_-$*

$$\frac{\sigma^2}{n} + \left[\frac{(n-1)\sigma^2}{2n\lambda_+} \left(1 - \frac{\|\mathbf{x}\|^2}{\lambda_-}\right)\right]^+ \leq \mathbb{E}\left[\frac{1}{n} \sum_{i=1}^n (w_i(t) - w^*)^2\right] \leq \frac{\sigma^2}{2\lambda_-} + \mathbb{E}[(\bar{w}_t - w^*)^2]$$

where $[\cdot]^+ \equiv \max(0, \cdot)$.

Theorem 3.3 says that average closeness of the noisy system to that of the noise-free optimum is controlled by the tradeoff between the noise and the coupling strength, and the number of circuit copies n . The former controls in large part the magnitude of the fluctuations, as discussed above. The latter quantity is

the unavoidable linear averaging component, and can be brought to zero only as fast as the law of large numbers allows, $\mathcal{O}(n^{-1/2})$ at best. For fixed n as $\lambda_-^{(n)} \rightarrow \infty$, the upper and lower bounds coincide since $\mathbb{E}[(\bar{w}(t) - w^*)^2] \rightarrow \sigma^2/n$. As both $n \rightarrow \infty$ and $\kappa \rightarrow \infty$ Theorem 3.3 confirms that $w_i(t) \rightarrow w^*$ in expectation. If the fluctuations are not made small however, linear averaging will be wrong, and the error will of course be greater. Just how bad linear averaging is when the fluctuations are allowed to be large is described in large part by the maximum curvature of the noise-free dynamics.

Finally, we note that the estimates above depend on the number of samples m only through the norm of the examples \mathbf{x} , and it is reasonable to assume that this quantity may be appropriately normalized based on the maximum firing rates of neurons in the circuit. However, the requirement that the organism must collect m observations before learning can proceed is not essential. We may also consider the *online* learning setting, where data are observed sequentially and updates to the parameters $(w)_i$ are made separately on the basis of each observation in temporal order. The analysis above studies convergence to and distance from the solution in the steady state, whatever that solution may be, given m pieces of evidence. Thus the online setting can also be considered as long as the time between observations is longer than the transient periods. Indeed, in many scenarios learning and decision making processes in the brain can take place on short time scales relative to the time scale on which experience is accumulated. In this case when another data point arrives, the system moves to a region defined (stochastically) around a new steady-state. A complication does arise when the new point arrives during the transient period of the previous learning process – before the system has had a chance to settle, on average, into the new equilibrium – however we do not attempt to model this situation here.

4 Discussion

The estimates given in Section 3 quantify the tradeoff between synchronization strength and ambient neuronal noise and the role this tradeoff plays in determining uncertainty of a function learned by way of a stochastic, nonlinear gradient dynamics adhering to a good standard of biological realism. Estimates both in expectation and in probability were derived. We showed how and where both the coupling strength and the topology of the network of neural ensembles impact the extent to which the noise, and therefore uncertainty, can be controlled.

We note that if the dynamics of a stochastic system are contracting, or can be made contracting with feedback, then combinations (e.g. parallel, serial, hierarchical) of such systems will be contracting (Pham et al., 2009; Lohmiller and Slotine, 1998). In the present setting, the system governing the fluctuations about the mean trajectory was contracting with a rate dependent on the coupling strength and the noise variance.

Although we have assumed diffusive couplings (implemented by gap-junctions for example, in the context of modeling the detailed behavior of neural populations), this need not be seen as a strong restriction: as discussed above in the context of network topology, quorum sensing can often provide for communication among neurons which, at an appropriate scale, might be reasonably modeled as diffusive interactions. Furthermore, dynamics in the computation of the quorum variable itself, when appropriate for modeling purposes, does not necessarily pose any special difficulty for establishing synchronization properties if virtual systems are used (Russo and Slotine, 2010).

More generally however we seek to address the precise meaning of ensemble measurements and population codes, as well as the information these codes convey about the underlying dynamics and signals. The results derived above support the notion that synchronization plays a more functional role in the context of learning processes in the brain, rather than being a mere epiphenomenon. Synchronization has been suggested, over a diverse history of experimental work, as a fundamental mechanism for improvement in precision and reduction in uncertainty in the nervous system (see e.g. (Needleman et al., 2001; Enright, 1980)). In retinal ganglion cells (Croner et al., 1993) and heart cells (Clay and DeHaan, 1979) the spatial mean across coupled cells cancels out noise. Populations of hair cells in otoliths perform redundant, collaborative computations to achieve robustness (Kandel et al., 2000; Eliasmith and Anderson, 2004).

Ensemble measurements have also been connected to behavior and have been suggested as inputs to brain-machine interfaces, while in stochastic neural decision making it has been suggested that it is the collective behavior across multiple populations of neurons that is responsible for perception and decision making, rather than activity of a single neuron or population of neurons (Gigante et al., 2009). Although generic networks

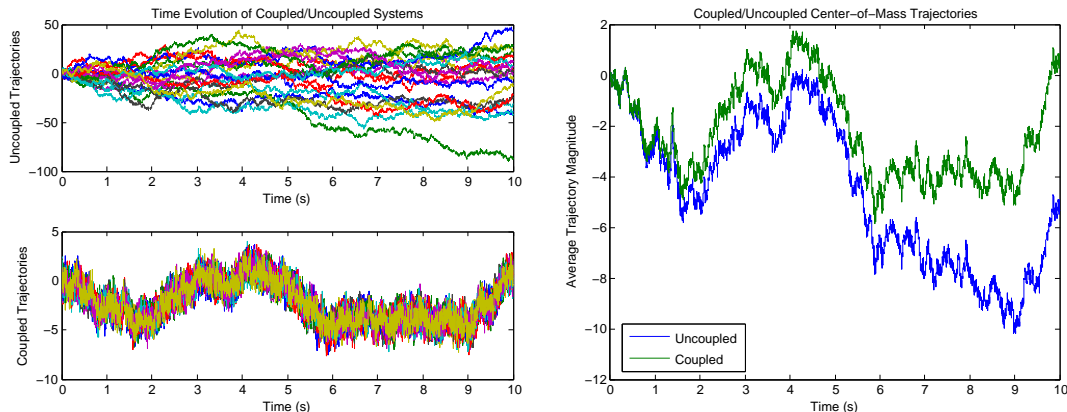


Figure 2: (Left) Simulated trajectories for coupled and uncoupled networks driven by the same noise. (Right) Population average trajectories for the coupled and uncoupled systems.

of neurons can be said to communicate predominantly using chemical signals, the stochastic system (3) can also be interpreted as capturing and modeling macro phenomena such as local field potentials (LFPs) in addition to specific networks of electrically coupled cells. In the context of LFPs, learning and decision making in the presence of uncertainty becomes a fundamentally important concept. This uncertainty can be seen to arise from three distinct sources. The approach discussed here treats the first two: intrinsic (neuronal) noise and noise in the form of possible measurement error. A third and equally important source of error is that of uncertainty in the inference process itself (Yang and Shadlen, 2007; Kiani and Shadlen, 2009). This uncertainty is specific to and inherent in the decision problem and is characterized by the posterior distribution over decisions given the experiential evidence. Our work only considers uncertainty beyond that of the inference process, and as such is one part of a larger puzzle. We argue that intrinsic noise is both experimentally and theoretically important – and involved enough technically – to be addressed in isolation, while holding all other variables constant. Indeed, intrinsic noise intensities can be large (in retinal cells for example (Croner et al., 1993)). The role of the network’s topology and coupling mechanism also strongly influences the overall picture, often in surprising or subtle ways. But it is also possible that the methods recruited here can be applied towards understanding some aspect of the inference error if different inferences from the same observations can be made by different “expert” (circuits) each with their own biases. Then averaging, nonlinearity and the uncertainty could potentially be treated in a similar framework.

5 Simulations

To empirically test the estimates given in Section 3 we simulated several systems of SDEs given by Equation (4) using Euler-Maruyama integration (over time $t \in [0, 10s]$, 10^5 regularly spaced sample points), for different settings of the parameters n (number of circuits or elements), κ (coupling strength) and σ (noise standard deviation). Initial conditions were randomly drawn from the uniform distribution on $[-5, 5]$, and we fixed $\|x\|^2 = 1$ and the coupling arrangement to all-to-all coupling with fixed strength determined by κ . For simplicity the simulated systems had equilibrium point at zero, corresponding to $y = 0$, so that $\langle x, y \rangle = 0$ and $X^* = w^*$ (the change of variables is the identity map and we can identify X_t with w_t).

For comparison purposes we first show on the left in Figure 2 typical simulated trajectories of uncoupled (top) and coupled (bottom) populations when $n = 20, \kappa = 5, \sigma = 10$. Both populations are driven by the same noise and the same set of initial conditions, however each element is driven by noise independent from the others as assumed above. From the units on the vertical axes, one can see that coupling clearly reduces inter-trajectory fluctuations as expected. On the right in Figure 2, we show the coupled/uncoupled populations’ respective center of mass trajectories for this particular simulation instance. One can see from this figure that the average of the coupled system tends closer to zero (X^*), and is less affected by large noise excursions.

To empirically test tightness of the estimates given in Section 3, we repeated simulations of each respec-

Quantity	Lower Bound	Simulated	Upper Bound
$\mathbb{E}\ \tilde{X}_t\ ^2$	9.405	9.497 (std= 3.1)	9.500
$\text{var}(\ \tilde{X}_t\ ^2)$	-	9.450 (std= 14.7)	111.046
$\frac{1}{n}\mathbb{E}\ X_t - X^*\mathbf{1}\ ^2$	5.470	12.249 (std= 22.2)	12.249 (std= 22.2)

Table 1: Estimates vs. simulated quantities: $n = 20, \kappa = 5, \sigma = 10$.

Quantity	Lower Bound	Simulated	Upper Bound
$\mathbb{E}\ \tilde{X}_t\ ^2$	11.281	11.719 (std= 3.8)	11.875
$\text{var}(\ \tilde{X}_t\ ^2)$	-	14.261 (std= 23.0)	184.45
$\frac{1}{n}\mathbb{E}\ X_t - X^*\mathbf{1}\ ^2$	1.814	1.933 (std= 2.5)	1.946 (std= 2.4)

Table 2: Estimates vs. simulated quantities: $n = 20, \kappa = 1, \sigma = 5$.

Quantity	Lower Bound	Simulated	Upper Bound
$\mathbb{E}\ \tilde{X}_t\ ^2$	45.125	47.053 (std= 15.2)	47.500
$\text{var}(\ \tilde{X}_t\ ^2)$	-	230.275 (std= 373.4)	2951.234
$\frac{1}{n}\mathbb{E}\ X_t - X^*\mathbf{1}\ ^2$	7.256	14.761 (std= 24.1)	14.784 (std= 24.1)

Table 3: Estimates vs. simulated quantities: $n = 20, \kappa = 1, \sigma = 10$.

Quantity	Lower Bound	Simulated	Upper Bound
$\mathbb{E}\ \tilde{X}_t\ ^2$	49.005	49.556 (std= 7.0)	49.500
$\text{var}(\ \tilde{X}_t\ ^2)$	-	49.332 (std= 70.6)	2598
$\frac{1}{n}\mathbb{E}\ X_t - X^*\mathbf{1}\ ^2$	1.490	1.449 (std= 1.6)	1.449 (std= 1.6)

Table 4: Estimates vs. simulated quantities: $n = 100, \kappa = 1, \sigma = 10$.

Quantity	Lower Bound	Simulated	Upper Bound
$\mathbb{E}\ \tilde{X}_t\ ^2$	9.880	10.137 (std= 1.5)	9.900
$\text{var}(\ \tilde{X}_t\ ^2)$	-	2.151 (std= 3.2)	102.362
$\frac{1}{n}\mathbb{E}\ X_t - X^*\mathbf{1}\ ^2$	1.099	1.496 (std= 1.5)	1.496 (std= 1.5)

Table 5: Estimates vs. simulated quantities: $n = 100, \kappa = 5, \sigma = 10$.

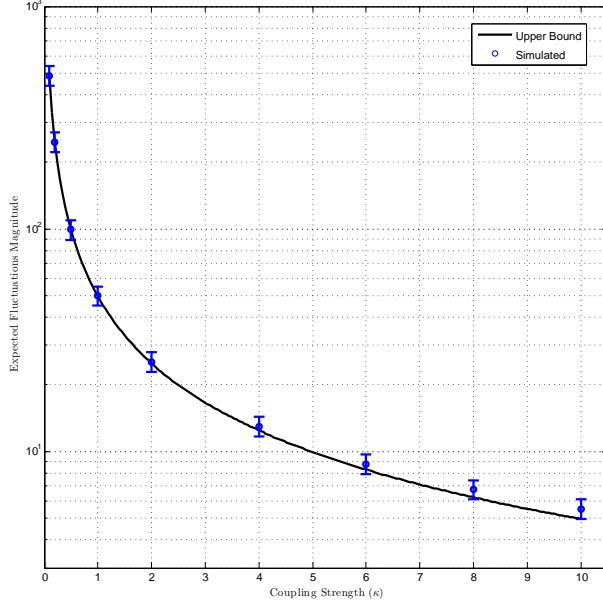


Figure 3: *Simulated vs. theoretical upper bound estimates of the fluctuations' expected magnitude over a range of coupling strengths κ . Here $n = 200$ neurons and $\sigma = 10$.*

tive system 5000 times, and averaged the relevant outcomes to approximate the expectations appearing in the bounds. Transient periods were excluded in all cases. In Tables 1 through 5 we show the values predicted by the bounds and the corresponding simulated quantities, for each respective triple of system parameter settings. Sample standard deviations of the simulated averages (expectations) are given in parentheses. In Figure 3 we show theoretical versus simulated expected magnitudes of the fluctuations $\mathbb{E}\|\dot{X}_t\|^2$ when $n = 200$ and $\sigma = 10$ over a range of coupling strengths. The solid dark trace is the upper bound of Theorem 3.1, while the open circles are the average simulated quantities (again 5000 separate simulations were run for each κ). Error bars are also given for the simulated expectations. Note that the magnitude scale (y -axis) is logarithmic, so the error bars are also plotted on a log scale. We omitted the lower theoretical bound from the plot because it is too close to the upper bound to visualize well relative to the scale of the bounds.

Generally, the estimates relating to the magnitude of the fluctuations are seen to be tight, and the variance estimate is within an order of magnitude. For the experiments with large noise amplitudes, the empirical estimates can appear to slightly violate the bounds where the bounds are tight since the variance across simulations is large. The lower bound estimating the distance of the center of mass to the noise-free solution is also seen to be reasonably good. For comparison, we give the upper estimate where the empirical distance is substituted in place of the expectation in order to show closeness to the lower bound. Theorem 3.3 predicts that the upper and lower estimates will eventually coincide if κ and/or n are chosen large enough.

6 Proofs

In this section we provide proofs of the results discussed in Section 3.

We first introduce a key Lemma to be used in the development immediately below.

Lemma 6.1. *Let $P = I - (1/n)\mathbf{1}\mathbf{1}^\top$, the canonical projection onto the zero mean subspace of \mathbb{R}^n . Then for all $x \in \mathbb{R}^n$*

$$0 \leq \langle Px, \tanh(x) \rangle \leq \|Px\|^2,$$

where the hyperbolic tangent applies elementwise.

Proof. Given $x \in \mathbb{R}^n$, define the index sets $I = \{1, \dots, n\}$, $I_+ = \{i \in I \mid (Px)_i \geq 0\}$, and $I_- = I \setminus I_+$. Since Px is zero mean, $\sum_{i \in I_+} (Px)_i = \sum_{i \in I_-} |(Px)_i|$. We will express the hyperbolic tangent as

$\tanh(z) = 2s(2z) - 1$, where $s(z) = (1 + e^{-z})^{-1}$ is the logistic sigmoid function. If we let $\mu = \frac{1}{n} \mathbf{1}^\top x$ be the center of mass of x , $(Px)_i = x_i - \mu \geq 0$ implies $s(x_i) \geq s(\mu)$ by monotonicity of s . Likewise, $(Px)_i < 0$ implies $s(x_i) < s(\mu)$. Finally, note that since $P^2 = P$ and $\mathbf{1} \in \ker P$, $\langle Px, \tanh(x) \rangle = \langle Px, P(2s(2x) - \mathbf{1}) \rangle = 2\langle Px, s(2x) \rangle$. Using these facts, we prove the lower bound first:

$$\begin{aligned} \langle Px, \tanh(x) \rangle &= 2 \sum_{i \in I_+} (Px)_i s(2x_i) - 2 \sum_{i \in I_-} |(Px)_i| s(2x_i) \\ &\geq 2s(2\mu) \sum_{i \in I_+} (Px)_i - 2s(2\mu) \sum_{i \in I_-} |(Px)_i| \\ &= 2s(2\mu) \cdot 0 = 0. \end{aligned}$$

Turning to the upper bound, we prove the equivalent statement $\langle Px, s(2x) - x \rangle \leq 0$. First, if $\mu = 0$, then $Px = x$ so $\langle Px, \tanh(x) \rangle = \langle x, \tanh(x) \rangle \leq \|x\| \|\tanh(x)\| \leq \|x\|^2 = \|Px\|^2$, since $\|\tanh(x)\| \leq \|x\|$ by virtue of the fact that $|\tanh(z)| = \tanh(|z|) \leq |z|$ for any $z \in \mathbb{R}$. Now suppose that $\mu > 0$. If $z \geq \mu > 0$, we can upper bound $s(2z)$ by the line tangent to the point $(\mu, s(2\mu))$: $s(2z) \leq mz + b$ with $m < \frac{1}{2}$ and $b > \frac{1}{2}$. If $z < \mu$, we can take the lower bound $s(2z) > \frac{1}{2}z + \frac{1}{2}\mu - s(2\mu)$. Using these estimates, we have that

$$\begin{aligned} \langle Px, s(2x) - x \rangle &= \sum_{i \in I_+} (Px)_i (s(2x_i) - x_i) + \sum_{i \in I_-} |(Px)_i| (x_i - s(2x_i)) \\ &\leq \sum_{i \in I_+} (Px)_i (b - (1 - m)x_i) + \sum_{i \in I_-} |(Px)_i| (\frac{1}{2}x_i + \frac{1}{2}\mu - s(2\mu)) \\ &\leq \sum_{i \in I_+} (Px)_i (b - (1 - m)\mu) + \sum_{i \in I_-} |(Px)_i| (\frac{1}{2}\mu + \frac{1}{2}\mu - s(2\mu)) \\ &= \left(\sum_{i \in I_+} (Px)_i \right) (b + m\mu - s(2\mu)) = 0. \end{aligned}$$

The second inequality follows from the fact that $(1 - m) > 0$, $x_i \geq \mu$ for $i \in I_+$ and $x_i < \mu$ for $i \in I_-$. Since $\sum_{i \in I_+} (Px)_i = \sum_{i \in I_-} |(Px)_i|$, and recalling that by definition b satisfies $m\mu + b = s(2\mu)$, the final equalities follow. If $\mu < 0$, then the proof is similar, taking the line tangent to the point $(\mu, s(2\mu))$ as a lower bound for $s(2z)$ and the line $\frac{1}{2}(z - \mu) + s(2\mu)$ as an upper bound. \square

6.1 Fluctuations Estimates: Proof of Theorem 3.1

We begin by adding $\lambda \|X_t\|^2 dt$, with $\lambda \in (0, \infty)$, to both sides of Equation (7) to obtain

$$\begin{aligned} \frac{1}{2} d\|\tilde{X}_t\|^2 + \lambda \|\tilde{X}_t\|^2 dt &= -\|\mathbf{x}\|^2 \langle \tanh X_t, \tilde{X}_t \rangle dt + (\lambda \|\tilde{X}_t\|^2 - \langle LX_t, \tilde{X}_t \rangle) dt \\ &\quad + \frac{1}{2} (n - 1) \tilde{\sigma}^2 dt + \tilde{\sigma} \|\tilde{X}_t\| dB_t = e^{-2\lambda t} d\left(\frac{1}{2} \|\tilde{X}_t\|^2 e^{2\lambda t}\right), \end{aligned}$$

where the second equality follows noticing that the right hand side is the total Ito derivative of the left hand side of the first equality. Now multiply both sides by $e^{2\lambda t}$, switch to integral form, and multiply both sides by $e^{-2\lambda t}$ to arrive at

$$\begin{aligned} \frac{1}{2} \|\tilde{X}_t\|^2 &= e^{-2\lambda t} \|\tilde{X}_0\|^2 + \int_0^t e^{2\lambda(s-t)} \left(\frac{1}{2} (n - 1) \tilde{\sigma}^2 - \|\mathbf{x}\|^2 \langle \tanh X_s, \tilde{X}_s \rangle \right) ds \\ &\quad + \int_0^t e^{2\lambda(s-t)} (\lambda \|\tilde{X}_s\|^2 - \langle LX_s, \tilde{X}_s \rangle) ds + \tilde{\sigma} \int_0^t e^{2\lambda(s-t)} \|\tilde{X}_s\| dB_s. \end{aligned} \tag{9}$$

Upper Bound: Next, note that $\langle LX_t, \tilde{X}_t \rangle = \langle L\tilde{X}_t, \tilde{X}_t \rangle$ since $L(\bar{X}_t \mathbf{1}) = 0$, and that \tilde{X}_t is by definition orthogonal to any constant vector. For all t we also have that

$$\begin{aligned} \lambda_- \|\tilde{X}_t\|^2 - \langle L\tilde{X}_t, \tilde{X}_t \rangle &\leq 0 \\ -\langle \tanh X_t, \tilde{X}_t \rangle &\leq 0 \end{aligned} \tag{10}$$

almost surely. The first inequality follows from the fact that for all $x \in \text{im } P$,

$$\lambda_- \|\tilde{X}_t\|^2 \leq \langle L\tilde{X}_t, \tilde{X}_t \rangle \leq \lambda_+ \|\tilde{X}_t\|^2,$$

if λ_- is the Fiedler eigenvalue of L and λ_+ is the largest eigenvalue of L . The second inequality is given by Lemma 6.1. Setting $\lambda \equiv \lambda_-$ and applying the inequalities (10) to Equation (9) gives the estimate

$$\begin{aligned} \frac{1}{2} \|\tilde{X}_t\|^2 &\leq e^{-2\lambda_- t} \|\tilde{X}_0\|^2 + \frac{(n-1)\tilde{\sigma}^2}{2} \int_0^t e^{2\lambda_-(s-t)} ds + \tilde{\sigma} \int_0^t e^{2\lambda_-(s-t)} \|\tilde{X}_s\| dB_s \\ &= e^{-2\lambda_- t} \|\tilde{X}_0\|^2 + \frac{(n-1)\tilde{\sigma}^2}{4\lambda_-} (1 - e^{-2\lambda_- t}) + \tilde{\sigma} \int_0^t e^{2\lambda_-(s-t)} \|\tilde{X}_s\| dB_s \end{aligned} \quad (11)$$

almost surely. Taking expectations and noting that $\mathbb{E} \left[\int_0^t e^{2\lambda_-(s-t)} \|\tilde{X}_s\| dB_s \right] = 0$, we have that

$$\mathbb{E} \|\tilde{X}_t\|^2 \leq \frac{(n-1)\tilde{\sigma}^2}{2\lambda_-} \quad (12)$$

after transients of rate $2\lambda_-$.

Lower Bound: We show that $\mathbb{E} \|\tilde{X}_t\|^2$ has a lower bound that can also be expressed in terms of the coupling strength and the noise level. The derivation is similar to that of the upper bound, and we begin with Equation (9). We set $\lambda \equiv \lambda_+$ and apply the estimates $\lambda_+ \|\tilde{X}_s\|^2 - \langle L\tilde{X}_s, \tilde{X}_s \rangle \geq 0$ and $\langle \tanh X_s, \tilde{X}_s \rangle \leq \|\tilde{X}_s\|^2$ for all s a.s., yielding

$$\frac{1}{2} \|\tilde{X}_t\|^2 \geq e^{-2\lambda_+ t} \|\tilde{X}_0\|^2 + \int_0^t e^{2\lambda_+(s-t)} \left(\frac{1}{2} (n-1)\tilde{\sigma}^2 - \|\mathbf{x}\|^2 \|\tilde{X}_s\|^2 \right) ds + \tilde{\sigma} \int_0^t e^{2\lambda_+(s-t)} \|\tilde{X}_s\| dB_s.$$

Taking expectations and integrating the Ito term, we have

$$\frac{1}{2} \mathbb{E} \|\tilde{X}_t\|^2 \geq e^{-2\lambda_+ t} \mathbb{E} \|\tilde{X}_0\|^2 + \frac{(n-1)\tilde{\sigma}^2}{4\lambda_+} (1 - e^{-2\lambda_+ t}) - \|\mathbf{x}\|^2 \int_0^t e^{2\lambda_+(s-t)} \mathbb{E} \|\tilde{X}_s\|^2 ds.$$

After transients of rate $2\lambda_-$, we can apply (12) to estimate the remaining integral and lower bound the above equation by

$$e^{-2\lambda_+ t} \mathbb{E} \|\tilde{X}_0\|^2 + \frac{(n-1)\tilde{\sigma}^2}{4\lambda_+} (1 - e^{-2\lambda_+ t}) - \|\mathbf{x}\|^2 \frac{(n-1)\tilde{\sigma}^2}{4\lambda_- \lambda_+} (1 - e^{-2\lambda_+ t}).$$

Since $\lambda_- \leq \lambda_+$, transients of rate $2\lambda_+$ have already transpired if we suppose that we have waited for transients of rate $2\lambda_-$. Therefore, we can say that after transients of rate $2\lambda_-$,

$$\mathbb{E} \|\tilde{X}_t\|^2 \geq \frac{(n-1)\tilde{\sigma}^2}{2\lambda_+} \left(1 - \frac{\|\mathbf{x}\|^2}{\lambda_-} \right). \quad (13)$$

6.1.1 Inverting the change of variables

Finally, we can obtain corresponding upper and lower bounds for the original system (3) noting that since $\tilde{X}_t = P(\mathbf{w}(t)\|\mathbf{x}\|^2 - \langle \mathbf{x}, \mathbf{y} \rangle \mathbf{1}) = \|\mathbf{x}\|^2 P\mathbf{w}(t)$, we have $\mathbb{E} \|\tilde{\mathbf{w}}\|^2 = \mathbb{E} \|\tilde{X}_t\|^2 / \|\mathbf{x}\|^4$, where we have used the notation $\tilde{\mathbf{w}}$ for $P\mathbf{w}$. The $\|\mathbf{x}\|^4$ in the denominator then cancels with the same quantity occurring in $\tilde{\sigma}^2$ in Equations (12) and (13), giving the final form shown in Theorem 3.1.

6.2 Fluctuations Estimates: Proof of Theorem 3.2

We first derive the fourth moment of the norm of the fluctuations. Starting from Equation (11), allow transients of rate $2\lambda_-$ to pass so that we are left with the integral inequality

$$\frac{1}{2} \|\tilde{X}_t\|^2 \leq \frac{(n-1)\tilde{\sigma}^2}{4\lambda_-} + \tilde{\sigma} \int_0^t e^{2\lambda_-(s-t)} \|\tilde{X}_s\| dB_s.$$

Squaring both sides, we can apply the identity $(a + b)^2 \leq 2a^2 + 2b^2$ to obtain

$$\|\tilde{X}_t\|^4 \leq \left(\frac{(n-1)\tilde{\sigma}^2}{\sqrt{2}\lambda_-} \right)^2 + 8\tilde{\sigma}^2 \left(\int_0^t e^{2\lambda_-(s-t)} \|\tilde{X}_s\| dB_s \right)^2.$$

Taking expectations and invoking Ito's Isometry for the second term leads to

$$\begin{aligned} \mathbb{E}\|\tilde{X}_t\|^4 &\leq \left(\frac{(n-1)\tilde{\sigma}^2}{\sqrt{2}\lambda_-} \right)^2 + 8\tilde{\sigma}^2 \int_0^t e^{4\lambda_-(s-t)} \mathbb{E}\|\tilde{X}_s\|^2 ds \\ &\leq \left(\frac{(n-1)\tilde{\sigma}^2}{\sqrt{2}\lambda_-} \right)^2 + \frac{8\tilde{\sigma}^2}{4\lambda_-} \left(\frac{(n-1)\tilde{\sigma}^2}{2\lambda_-} \right) = \left(\frac{(n-1)\tilde{\sigma}^2}{2\lambda_-} \right)^2 \left(2 + \frac{4}{n-1} \right) \end{aligned}$$

where the estimate (12) has been substituted in for $\mathbb{E}\|\tilde{X}_s\|^2$. An upper bound on the variance is then obtained from the identity $\text{var}(Z^2) = \mathbb{E}[Z^4] - (\mathbb{E}Z^2)^2$ and the lower estimate given in Equation (13). Reversing the change of variables as in Section 6.1.1 yields the final result.

6.3 Distance to the Noise-Free Trajectory: Proof of Theorem 3.3

Theorem 3.1 can be applied towards providing a lower bound for the average distance between the noisy trajectories of the neural circuit and the noise-free solution to the learning problem. First observe that from the orthogonal decomposition $X_t = PX_t + QX_t$ and the change of variables mapping (3) to (4),

$$\|X_t\|^2 = \|\bar{X}_t \mathbf{1}\|^2 + \|\tilde{X}_t\|^2 = \|\mathbf{x}\|^4 \|\mathbf{w} - w^* \mathbf{1}\|^2. \quad (14)$$

Furthermore, we have that

$$\bar{X}_t = n^{-1} \sum_i X_i(t) = n^{-1} \sum_i (w_i \|\mathbf{x}\|^2 - \langle \mathbf{x}, \mathbf{y} \rangle),$$

so evidently $\|\mathbf{x}\|^{-4} \mathbb{E} \bar{X}_t^2 = \mathbb{E}[(\bar{w}_t - w^*)^2]$. Next, note that if the fluctuations are small, the trajectories $(w_i(t))_{i=1}^n$ are close to one another and the average trajectory $\bar{w}_t = n^{-1} \mathbf{w}(t)^\top \mathbf{1}$ evolves essentially as $\bar{w}_t \sim w^* + \frac{\sigma}{\sqrt{n}} W_t$, where W_t is interpreted as a white noise process. In this case we then have that $\mathbb{E}[(\bar{w}_t - w^*)^2] = \frac{\sigma^2}{n}$, and we see that $\mathbb{E}[(\bar{w}_t - w^*)^2] \geq \frac{\sigma^2}{n}$ when the fluctuations are not necessarily small. So we have that $\|\mathbf{x}\|^{-4} \mathbb{E} \bar{X}_t^2 \geq \frac{\sigma^2}{n}$. Combining the above with Theorem 3.1,

$$\frac{\sigma^2}{n} + \left[\frac{(n-1)\sigma^2}{2n\lambda_+} \left(1 - \frac{\|\mathbf{x}\|^2}{\lambda_-} \right) \right]^+ \leq \frac{\mathbb{E} \bar{X}_t^2}{\|\mathbf{x}\|^4} + \frac{\mathbb{E} \|\tilde{X}_t\|^2}{n\|\mathbf{x}\|^4} \leq \frac{\sigma^2}{2\lambda_-} + \mathbb{E}[(\bar{w}_t - w^*)^2]$$

with the notation $[\cdot]^+ \equiv \max(0, \cdot)$. Equation (14) then shows that the middle quantity above is equal to $\mathbb{E} \left[\frac{1}{n} \sum_{i=1}^n (w_i(t) - w^*)^2 \right]$.

Acknowledgments

The authors acknowledge helpful suggestions from and discussions with Jonathan Mattingly. JB gratefully acknowledges support under NSF contract IIS-08-03293, ONR contract N000140710625 and Alfred P. Sloan Foundation grant no. BR-4834 to M. Maggioni.

References

- Adams, P. (1998). Hebb and darwin. *Journal of Theoretical Biology*, 195(4):419–438.
- Bennett, M. and Zukin, R. (2004). Electrical coupling and neuronal synchronization in the mammalian brain. *Neuron*, 41(4):495–511.

- Cao, M., Stewart, A., and Leonard, N. (2010). Convergence in human decision-making dynamics. *Systems and Control Letters*, 59:87–97.
- Clay, J. R. and DeHaan, R. L. (1979). Fluctuations in interbeat interval in rhythmic heart-cell clusters. role of membrane voltage noise. *Biophysical Journal*, 28(3):377–389.
- Croner, L. J., Purpura, K., and Kaplan, E. (1993). Response variability in retinal ganglion cells of primates. *Proceedings of the National Academy of Sciences of the United States of America*, 90(17):8128–8130.
- Eliasmith, C. and Anderson, C. (2004). *Neural Engineering: Computation, Representation, and Dynamics in Neurobiological Systems*. MIT Press.
- Enright, J. (1980). Temporal precision in circadian systems: a reliable neuronal clock from unreliable components? *Science*, 209(4464):1542–1545.
- Faisal, A., Selen, L., and Wolpert, D. (2008). Noise in the nervous system. *Nat. Rev. Neurosci.*, 9:292–303.
- Fernando, C., Goldstein, R., and Szathmary, E. (2010). The neuronal replicator hypothesis. *Neural Computation*, 22(11):2809–2857.
- Fukuda, T., Kosaka, T., Singer, W., and Galuske, R. (2006). Gap junctions among dendrites of cortical gabaergic neurons establish a dense and widespread intercolumnar network. *J. Neurosci.*, 26(13):3434–3443.
- Gigante, G., Mattia, M., Braun, J., and Del Giudice, P. (2009). Bistable perception modeled as competing stochastic integrations at two levels. *PLoS Comput Biol*, 5(7):e1000430.
- Hahnloser, R., Douglas, R. J., Mahovald, M., and Hepp, K. (1999). Feedback interactions between neuronal pointers and maps for attentional processing. *Nat. Neurosci.*, 2:746–752.
- Hung, C., Kreiman, G., Poggio, T., and DiCarlo, J. (2005). Fast Readout of Object Identity from Macaque Inferior Temporal Cortex. *Science*, 310(5749):863–866.
- Itti, L. and Koch, C. (2001). Computational modelling of visual attention. *Nat. Rev. Neurosci.*, 2(3):194–203.
- Jadbabaie, A., Lin, J., and Morse, A. S. (2003). Coordination of groups of mobile autonomous agents using nearest neighbor rules. *IEEE Transactions on Automatic Control*, 48(6):988–1001.
- Kandel, E., Schwartz, J., and Jessell, T. (2000). *Principles of Neural Science (4th. ed.)*. McGraw-Hill.
- Kiani, R. and Shadlen, M. N. (2009). Representation of confidence associated with a decision by neurons in the parietal cortex. *Science*, 324(5928):759–764.
- Kopell, N. (2000). We got rhythm: Dynamical systems of the nervous system. *Notices of the AMS*, 47:6–16.
- Kopell, N. and Ermentrout, G. (1986). Symmetry and phase-locking in chains of weakly coupled oscillators. *Communications on Pure and Applied Mathematics*, 39:623–660.
- Lee, T. and Mumford, D. (2003). Hierarchical bayesian inference in the visual cortex. *J Opt Soc Am A: Opt Image Sci Vis*, 20(7):1434–1448.
- Lohmiller, W. and Slotine, J. (1998). On contraction analysis for non-linear systems. *Automatica*, 34:683–696.
- Mumford, D. (1992). On the computational architecture of the neocortex – II: The role of cortico-cortical loops. *Biol. Cyb.*, 66:241–251.
- Needleman, D. J., Tiesinga, P. H., and Sejnowski, T. J. (2001). Collective enhancement of precision in networks of coupled oscillators. *Physica D: Nonlinear Phenomena*, 155(3-4):324–336.
- Pham, Q.-C. and Slotine, J.-J. (2007). Stable concurrent synchronization in dynamic system networks. *Neural Networks*, 20(1):62–77.

- Pham, Q.-C., Tabareau, N., and Slotine, J.-J. (2009). A contraction theory approach to stochastic incremental stability. *IEEE Transactions on Automatic Control*, 54(4):816–820.
- Poulakakis, I., Scardovi, L., and Leonard, N. (2010). Coupled stochastic differential equations and collective decision making in the two-alternative forced-choice task. In *Proc. American Control Conference*.
- Rao, R. and Ballard, D. (1999). Predictive coding in the visual cortex: A functional interpretation of some extra-classical receptive-field effects. *Nat. Neurosci.*, 2:79–87.
- Russo, G. and Slotine, J.-J. (2010). Global convergence of quorum sensing networks. *Physical Review E*, 28.
- Sherman, A. and Rinzel, J. (1991). Model for synchronization of pancreatic beta-cells by gap junction coupling. *Biophysical Journal*, 59(3):547 – 559.
- Slotine, J.-J. E. and Li, W. (1991). *Applied Nonlinear Control*. Prentice-Hall.
- Tabareau, N., Slotine, J.-J., and Pham, Q.-C. (2010). How synchronization protects from noise. *PLoS Comput Biol*, 6(1):e1000637.
- Taylor, A., Tinsley, M. R., Wang, F., Huang, Z., and Showalter, K. (2009). Dynamical Quorum Sensing and Synchronization in Large Populations of Chemical Oscillators. *Science*, 323(5914):614–617.
- Wang, W. and Slotine, J. (2005). On partial contraction analysis for coupled nonlinear oscillators. *Biological Cybernetics*, 92(1):38–53.
- Yang, T. and Shadlen, M. N. (2007). Probabilistic reasoning by neurons. *Nature*, 447(7148):1075–1080.
- Yao, Y., Rosasco, L., and Caponnetto, A. (2007). On early stopping in gradient descent learning. *Constructive Approximation*, 26(2):289–315.
- Young, G., Scardovi, L., and Leonard, N. (2010). Robustness of noisy consensus dynamics with directed communication. In *Proc. American Control Conference*.